Creep rupture assessment of cyclically heated 3D pressure pipelines with volumetric defects using a direct numerical approach

Heng Peng [a,b], Yinghua Liu [b,*], Haofeng Chen [c]

[a] Institute of Nuclear and New Energy Technology, Tsinghua University, Beijing, 100084, China
[b] Department of Engineering Mechanics, AML, Tsinghua University, Beijing, 100084, China
[c] Department of Mechanical and Aerospace Engineering, University of Strathclyde, Glasgow, G1 1XJ, UK

ARTICLE INFO

Keywords:
Creep rupture limit
Creep rupture life
Defective pressure pipeline
Direct numerical approach

ABSTRACT

Creep rupture assessment is a significant issue in the field of high-temperature structural integrity. In this paper, the creep rupture assessment of 3D pressure pipelines with volumetric defects subjected to cyclic thermo-mechanical loadings is done using a direct numerical approach within the framework of stress compensation method (SCM). For calculation of creep rupture limit, an extended shakedown analysis scheme with yield strength correction is essentially performed, where the revised yield strength is determined as the minimum of the plastic yield strength and the creep rupture strength of material corresponding to a specified elevated temperature and rupture time. This direct numerical approach performs the creep rupture assessment by using the given creep rupture data of material rather than simulating the degenerative process of material based on creep damage constitutive equations under a specified loading history. The numerical approach is incorporated into commercial finite element software of Abaqus. Parametric studies on geometric dimensions of part-through slot affecting the creep rupture limit of 3D pressure pipelines with volumetric defects are conducted. Numerical results shown in this study indicate that the direct numerical approach accurately identifies the creep rupture limit boundary of the pressure pipeline, verified by the elastic-plastic cycle-by-cycle analysis. Failure mechanisms, such as local creep rupture, global creep rupture and global plastic rupture are detected under different loading combinations. These results give the helpful information for in-service integrity assessment of defective pressure pipelines at elevated temperature, and demonstrate the applicability and application prospect of the direct numerical approach in solving questions relevant to design or life assessment of other engineering structures.

1. Introduction

Pressure pipelines, as the common structural elements for conveying pressure medium, are widely used in nuclear power industry, petrochemical industry and fossil fired power plants, and generally operate under elevated temperature and high pressure environment. In the course of operation, due to environment corrosion and erosion, mechanical damage and surface cracks grinding, there are some local volumetric defects, namely part-through slots on the surface of pipeline. These defects weaken the load-carrying capacity and reduce the remaining life of pipeline, and even lead to severe leaks and explosions. Therefore, for the safe operation of industrial pipeline system, structural integrity assessment of defective pipelines under elevated temperature and high pressure conditions is essential. The existing standards and specifications for safety assessment of in-service pressure vessels with volumetric defects [1] give severe limitations and requirements to the allowable dimensions of volumetric defects. Many articles [2–5] have also reported the studies on effects of the dimensions of volumetric defects on the load-carrying capacity of pipelines under steady and cyclic loads. These standards and relevant research works, to some extents, provide the scientific and reasonable criteria and theoretical basis for the structural integrity assessment of defective pressure pipelines. However, these results are only based on the elastic-plastic analysis of pipeline under normal temperature condition and do not consider the creep rupture effect of pipeline under elevated temperature condition. Therefore, this research aims at the creep rupture assessment of pressure pipelines with volumetric defects under cyclic elevated temperature and high pressure, and attempts to make up the deficiency of present criteria

* Corresponding author.
E-mail address: yhliu@mail.tsinghua.edu.cn (Y. Liu).

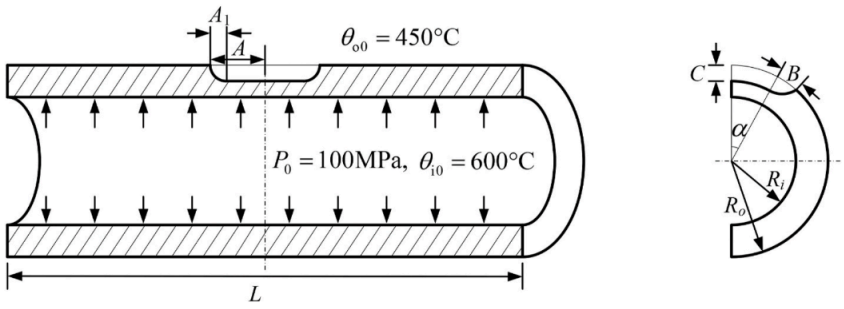

Fig. 1. Geometric sketch of a pressure pipeline with volumetric defect under internal pressure and cyclic temperature load.

Table 1
Geometric parameters of pressure pipelines with different sizes of part-through slots (mm).

Type of volumetric defect	R_o	R_i	L	α	A_1	A	B	C
Small area slot	21	17	250	0	2	2	2	2
Axial slot	21	17	250	0	2	16	2	2
Circumferential slot	21	17	250	45°	2	2	2	2
Large area slot	21	17	250	45°	2	16	2	2

and approaches for structural integrity assessment of defective pressure pipelines.

For a pressure vessel component operating at elevated temperature environment, not only the plastic deformation under instantaneous action but also the creep deformation under long-time action should be considered. Thus, both plastic failure and creep rupture are concerned for structural integrity assessment of pressure pipelines with defects. Creep rupture is interpreted as a situation that the cumulative creep damage reaches to a critical value. In general, the creep rupture analysis of a component can be performed by simulating the evolution of material deterioration under the given operating condition through creep damage models [6–8]. In recent years, some researchers [9–13] have conducted plastic failure analysis considering creep damage or creep rupture analysis to calculate the plastic limit load or ultimate creep load of pressure vessels with various volumetric defects at elevated temperature. It is noted that these numerical procedures require to conduct the full elastic-plastic creep analysis throughout the entire loading history and to know the detailed creep constitutive model and parameters. As reported in literature, this approach is mainly used for the high-temperature creep analysis at a certain constant temperature, because it is difficult to obtain a unified creep damage constitutive model and material parameters applying for all temperature conditions. These inelastic finite element (FE) calculations are usually tedious and time-consuming, especially for the cyclic loading condition. In addition, the corresponding parameters of creep constitutive model of a material are hard to get directly from creep experiment, and in most cases only creep rupture data are known.

The integrity assessment procedure R5 [14] and ASME NH [15] code provide some simplified methods of inelastic analysis for creep rupture assessment, where only the creep rupture data are used, rather than to conduct the complex cycle-by-cycle (CBC) elastic-plastic creep computation. Based upon the same method as R5, the shakedown analysis procedure of linear matching method (LMM) was extended for creep rupture prediction [16,17]. This method requires that the applied load of structure lies within the modified shakedown load boundary calculated by the shakedown analysis with yield strength correction. The modified yield strength is selected as the lower one of the creep rupture strength and the original yield strength. Based on the same theory as the creep rupture analysis procedure of LMM, the stress compensation method (SCM) recently proposed by authors was also developed for creep rupture assessment [18]. This approach does not need to conduct the CBC incremental elastic-plastic creep computation and essentially performs a shakedown analysis with yield strength correction, which can be considered as a direct numerical approach. The developed direct numerical approach within the SCM framework for creep rupture

Table 3
Material parameters of 316 stainless steel.

Parameter	Modulus of elasticity	Poisson ratio	Yield strength	Expansion coefficient
Value	195 GPa	0.31	445 MPa	1.8×10^{-5}

Table 2
Relationship between creep rupture strength [MPa] and temperature under different load holding times for 316 stainless steel.

Temperature [°C]	Time [h]										
	1	10	30	100	300	1×10^3	3×10^3	1×10^4	3×10^4	1×10^5	3×10^5
425	445	445	445	445	445	445	445	445	445	445	445
450	437	437	437	437	437	437	437	437	419	395	372
475	431	431	431	431	430	429	409	389	352	317	286
500	419	419	419	419	401	381	349	322	285	248	219
525	406	406	388	371	340	307	275	248	214	183	158
550	393	381	350	323	289	268	230	203	173	147	125
575	380	347	311	283	249	223	194	169	142	120	100
600	357	300	266	241	212	185	159	136	112	94	79
625	315	259	229	205	179	155	130	110	89	72	59
650	275	224	199	176	151	129	107	88	70	57	46
675	244	194	170	150	127	108	89	71	57	44	35
700	212	167	147	128	106	89	72	57	45	34	27
725	186	144	127	108	92	76	60	47	36	27	21
750	163	125	109	91	76	63	50	38	29	21	16
775	144	109	94	78	64	52	41	30	23	16	12
800	124	92	79	65	54	42	32	24	18	12	9

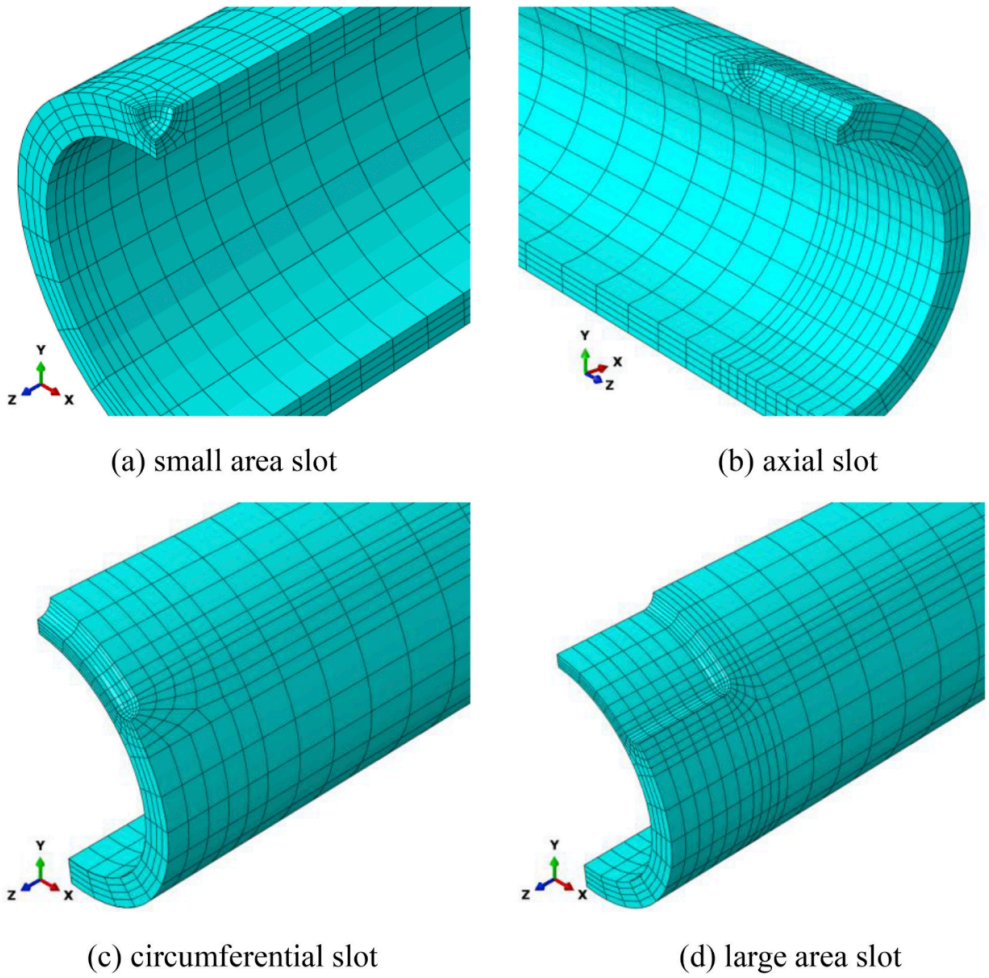

Fig. 2. FE meshes for pressure pipelines with four different types of part-through slots.

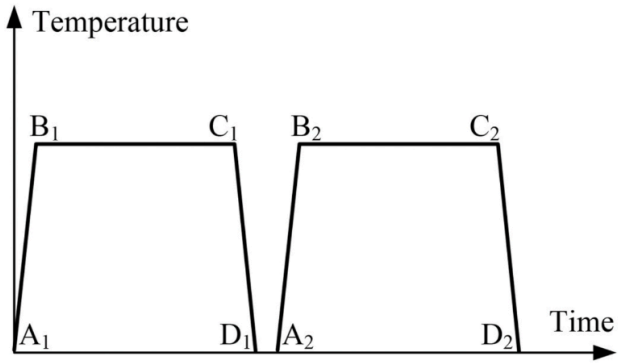

Fig. 3. Temperature history of the defective pressure pipeline.

assessment includes two numerical schemes which are respectively utilised for creep rupture life prediction and creep rupture limit calculation. The direct numerical approach was utilised for creep rupture analyses of a 3D holed plate and an engineering structure of pipe junction under cyclic loading condition, and showed good computational performance [18].

The objective of this work is to present the creep rupture assessment of cyclically heated 3D pressure pipelines with volumetric defects at elevated temperature using the direct numerical approach and to systematically investigate the effects of volumetric defects on the creep rupture limit load of pressure pipeline. The outline of this paper is as follows. Section 2 describes the direct numerical approach for creep rupture analysis. In Section 3, the FE models of pipeline with four types of part-through slots and the creep rupture data of material are introduced. The numerical results are presented and the effect of geometrical configuration of part-through slots on the creep rupture limit load of pressure pipeline at elevated temperature are discussed in Section 4. Finally, key conclusions are drawn in Section 5.

2. Direct numerical approach for creep rupture analysis

2.1. Theoretical aspect

We consider a structural body is subjected to the surface load $\lambda P(x_k, t)$ acting on the area S^P, the zero displacement boundary on the rest of area and the cyclic temperature field $\lambda\theta(x_k, t)$ operating within the body, where the load factor λ is used to scale the actual load. If the elastic mechanical stress history $\sigma_{ij}^P(x_k, t)$ under the surface load $P(x_k, t)$ and the elastic thermal stress history $\sigma_{ij}^\theta(x_k, t)$ under the temperature field $\theta(x_k, t)$ are solved, the linear elastic stress history $\lambda\sigma_{ij}^E(x_k, t)$ of the body under the applied thermal and mechanical loads can be obtained by the means

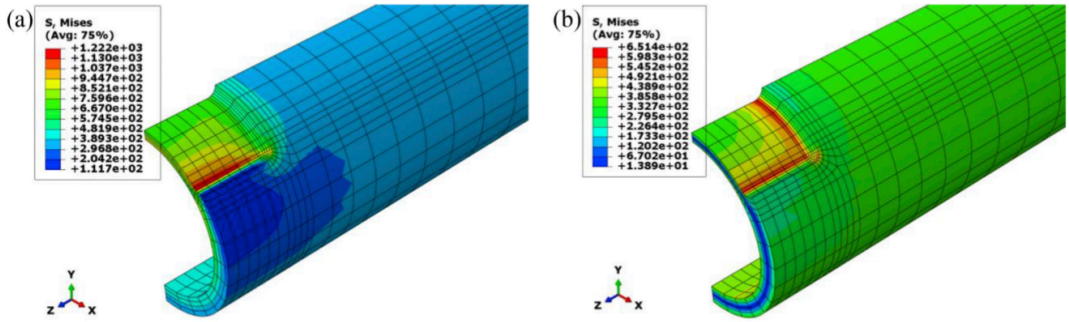

Fig. 4. FE solutions for the pressure pipeline with a large area slot under (a) reference inner pressure and (b) reference temperature load.

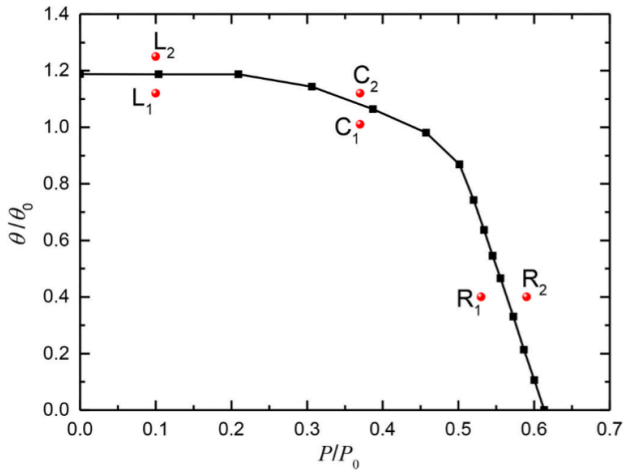

Fig. 5. Creep rupture limit interaction curve for the pressure pipeline with a large area slot under constant inner pressure and cyclic temperature load for the given creep rupture time 100 h.

of superposition principle:

$$\lambda\sigma_{ij}^{E}(x_k,t)=\lambda\sigma_{ij}^{P}(x_k,t)+\lambda\sigma_{ij}^{\theta}(x_k,t) \tag{1}$$

The material is assumed to be isotropic and elastic-perfectly plastic (EPP), and obeys von Mises yield rule. Under the action of cyclic mechanical and thermal loads, the cyclic stress response $\sigma_{ij}(x_k,t)$ of the elastoplastic structure is

$$\sigma_{ij}(x_k,t)=\lambda\sigma_{ij}^{E}(x_k,t)+\rho_{ij}(x_k)+\rho_{ij}^{r}(x_k,t) \tag{2}$$

where $\rho_{ij}^{r}(x_k,t)$ represents the varying residual stress over time and $\rho_{ij}(x_k)$ represents the time-independent residual stress. It is noted that for the shakedown condition the varying residual stress $\rho_{ij}^{r}(x_k,t)$ is equal to zero. Therefore, when the structure shakes down, its cyclic stress response becomes

$$\sigma_{ij}(x_k,t)=\lambda\sigma_{ij}^{E}(x_k,t)+\rho_{ij}(x_k) \tag{3}$$

For a structural component operating at elevated temperature, the material points within the creep temperature range undergo creep deformation and damage, and therefore the failure of the structural component is time-dependent. The load-carrying capacity of the structural component is reduced when considering the creep rupture effect. To evaluate the load-carrying capacity of high-temperature structure, some researchers [16–20] have established a simplified creep analysis procedure based on the extended shakedown theory. Similar to the description of the classical shakedown theorem, the extended shakedown theorem for creep rupture analysis is re-stated as follows [18]:

For a creeping structural element, with volume V, under thermo-mechanical loading, it will not fail due to creep rupture over a time period, $t \le t_f$, if a time-independent residual stress field $\rho_{ij}(x_k)$ is found so that the cyclic stress response $\sigma_{ij}(x_k,t)$ satisfies the yield condition described in Eq. (4) at all material points $x_k \in V$ for arbitrary loading paths.

$$f\left(\sigma_{ij}(x_k,t),\sigma_y^{R}(t_f,x_k)\right)=f\left(\lambda\sigma_{ij}^{E}(x_k,t)+\rho_{ij}(x_k),\sigma_y^{R}(t_f,x_k)\right)\le 0 \tag{4}$$

where $\sigma_y^{R}(t_f,x_k)$ is the modified yield strength of each material point x_k under the given rupture time t_f. The modified yield strength $\sigma_y^{R}(t_f,x_k)$ is determined as the minimum of the plastic yield strength $\sigma_y(x_k)$ and the creep rupture strength $\sigma_C(t_f,\theta(x_k))$ of material corresponding to the given rupture time t_f and temperature $\theta(x_k)$, i.e.

$$\sigma_y^{R}(t_f,x_k)=\min\left\{\sigma_y(x_k),\sigma_C\left(t_f,\theta(x_k)\right)\right\} \tag{5}$$

Based on this theory, the evaluation of creep rupture limit load of a structure under the given rupture time is translated to calculate the maximum permissible load factor λ. It should be noted that the above theory applies to both the cyclic and monotonic loading conditions. The monotonic loading condition can be considered as a special case of cyclic loading condition, i.e., with one load vertex in a load cycle.

2.2. *Numerical scheme for the calculation of creep rupture limit*

The numerical scheme based on the SCM framework for calculation of creep rupture limit has been detailed in our previous works [18]. A brief overview of the numerical scheme is described in the rest of this section.

We consider that the loading history contains r load vertices, $\sigma_{ij}^{E}(x_k,t_l)$,$l=1,2,\cdots,r$. The yield condition described in Eq. (4) will be tested at r load vertices. The numerical scheme aims to search for a constant residual stress field $\rho_{ij}(x_k)$ to determine the maximum load factor λ. The numerical scheme contains two iterative loops. A sequence of iterative calculations of FE equilibrium equations are carried out in the inner loop to optimise the time-independent residual stress field and the load factor λ is updated through the use of an iterative control scheme in the outer loop to obtain the shakedown limit [18,21,22].

For the n-th iteration of inner loop.

1) Determine the total stress $\sigma_{ij}^{(n)}(x_k,t_l)$ at every gauss point for every load vertex

$$\sigma_{ij}^{(n)}(x_k,t_l)=\lambda^{(m)}\sigma_{ij}^{E}(x_k,t_l)+\rho_{ij}^{(n)}(x_k),l=1,2,\cdots,r \tag{6}$$

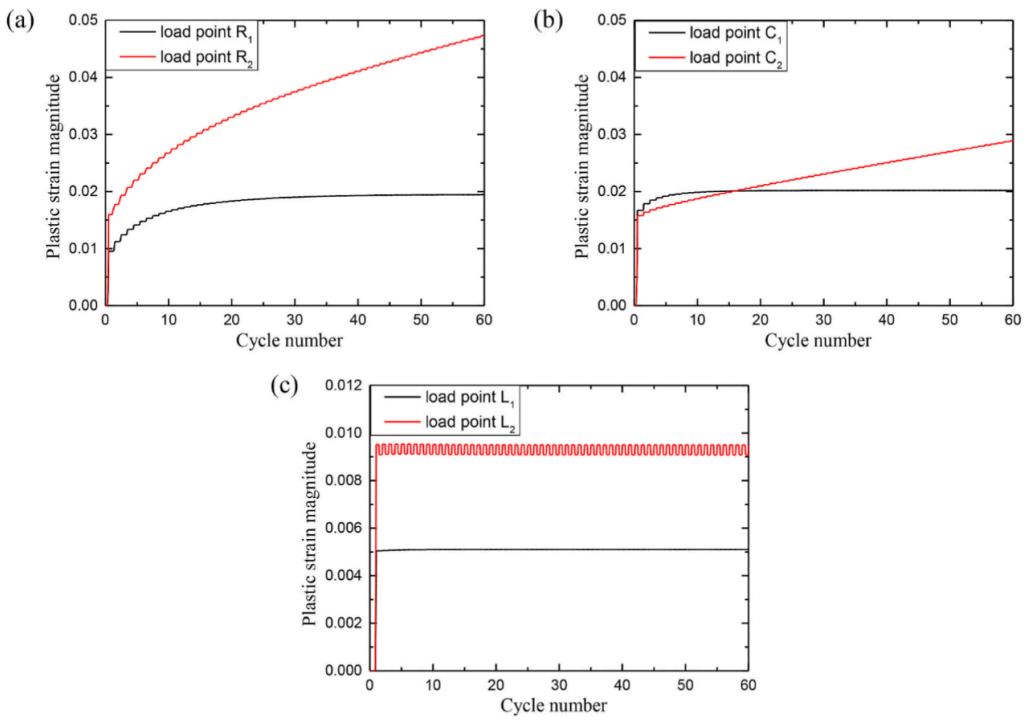

Fig. 6. Plastic strain magnitude histories of the pressure pipeline with a large area slot under the selected load points: (a) "R_1", "R_2"; (b) "C_1", "C_2"; (c) "L_1", "L_2"

2) Calculate the compensation stress $\sigma_{ij}^{C(n)}(x_k,t_l)$ at every gauss point for every load vertex

$$\sigma_{ij}^{C(n)}(x_k,t_l)=\xi^{(n)}(x_k,t_l)\cdot\sigma_{ij}^{(n)}(x_k,t_l)$$

$$\text{where } \xi^{(n)}(x_k,t_l)=\begin{cases}\dfrac{\overline{\sigma}^{(n)}(x_k,t_l)-\sigma_y^{R(n)}(t_f,x_k)}{\overline{\sigma}^{(n)}(x_k,t_l)} & \overline{\sigma}^{(n)}(x_k,t_l)>\sigma_y^{R(n)}(t_f,x_k)\\ 0 & \overline{\sigma}^{(n)}(x_k,t_l)\le\sigma_y^{R(n)}(t_f,x_k)\end{cases} \tag{7}$$

where $\sigma_y^{R(n)}(t_f,x_k)$ is determined by Eq. (5), and $\overline{\sigma}^{(n)}(x_k,t_l)$ is the von Mises stress of $\sigma_{ij}^{(n)}(x_k,t_l)$. It is noted that for the simplification of writing $\sigma_{ij}^{C(n)}(x_k,t_l)$ is written as $\sigma_{ij}^{C(n)}(t_l)$ or $\sigma_{pq}^{C(n)}(t_l)$, $\rho_{ij}^{(n)}(x_k)$ is written as $\rho_{ij}^{(n)}$, and $\sigma_{ij}^{E}(x_k,t_l)$ is written as $\sigma_{ij}^{E}(t_l)$ in the following text.

3) Solve the equations in Eq. (8), and then optimise the residual stress $\rho_{pq}^{(n+1)}$ via Eqs. (9) and (10) for the next iteration.

$$K_{st}\Delta u_t^{(n+1)}=\sum_{l=1}^{r}\left\{\lambda^{(m)}\int_V B_{spq}\left[\Delta\sigma_{pq}^{E}(t_l)+D_{pqij}\Delta\varepsilon_{ij}^{\theta}(t_l)\right]dV\right\}+\int_V B_{spq}\sigma_{pq}^{C(n)}(t_l)dV \tag{8}$$

$$\Delta\rho_{pq}^{(n+1)}=D_{pqij}B_{ijt}\Delta u_t^{(n+1)}-\lambda^{(m)}\sum_{l=1}^{r}\left[\Delta\sigma_{pq}^{E}(t_l)+D_{pqij}\Delta\varepsilon_{ij}^{\theta}(t_l)\right]-\sum_{l=1}^{r}\sigma_{pq}^{C(n)}(t_l) \tag{9}$$

$$\rho_{pq}^{(n+1)}=\rho_{pq}^{(n)}+\frac{1}{r}\Delta\rho_{pq}^{(n+1)} \tag{10}$$

4) Check the convergence of $\sigma_{pq}^{C(n)}(t_l)$ using Criterion (11).

$$\left|\xi^{(n+1)}(x_k,t_l)-\xi^{(n)}(x_k,t_l)\right|<\delta_1 \tag{11}$$

where δ_1 is a given error margin. If Criterion (11) is not satisfied, the process returns to Step 1, and then the next iteration of inner loop starts. Otherwise, the iteration of inner loop ends.

For the *m*-th iteration of outer loop.

1) Complete the calculation of inner loop.
2) Search for the maximum value of $\xi^{(n+1)}(x_k,t_l)$ among all the Gauss points and mark it as $\xi_{\max}^{(n+1)}$, i.e.

$$\xi_{\max}^{(n+1)}=\max\left\{\xi^{(n+1)}(x_k,t_l)\middle|x_k\in V,l=1,2,\cdots,r\right\} \tag{12}$$

3) If Condition (13) is satisfied,

$$\frac{\xi_{\max}^{(n+1)}}{\xi_{\max}^{(n)}}\le\delta_2,\ \text{and}\ \omega>0.1 \tag{13}$$

$\lambda^{(m+1)}$ is determined as

$$\lambda^{(m+1)}=\lambda^{(m)}\frac{1-\left(\omega\cdot\xi_{\max}^{(n+1)}\right)/2}{1-\omega\cdot\xi_{\max}^{(n+1)}} \tag{14}$$

where δ_2 and ω are parameters to control the convergence rate of load factors, and then $\omega=\omega/2$. Otherwise, $\lambda^{(m+1)}$ is determined as

$$\lambda^{(m+1)}=\lambda^{(m)}\left(1-\omega\cdot\xi_{\max}^{(n+1)}\right) \tag{15}$$

4) Check whether the yield conditions are met at all material points by

$$\xi_{\max}^{(n+1)}<\delta_3 \tag{16}$$

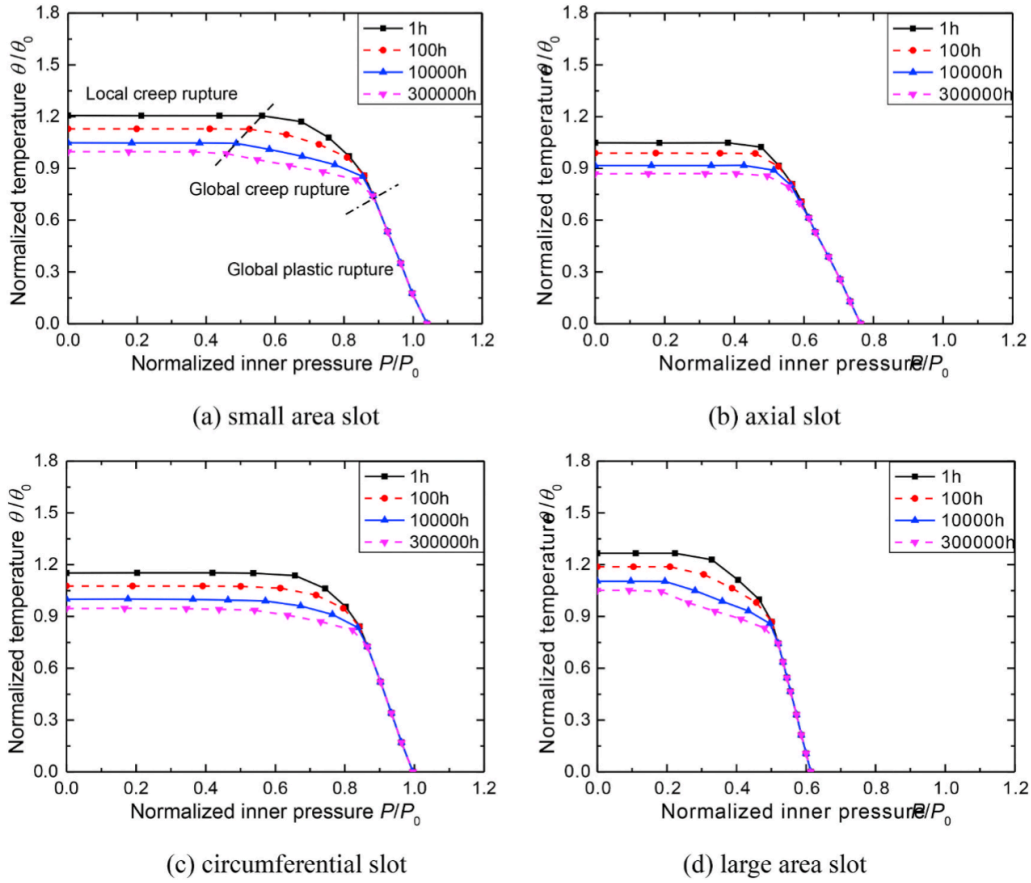

Fig. 7. Creep rupture limit interaction curves for the pressure pipelines with four types of part-through slots.

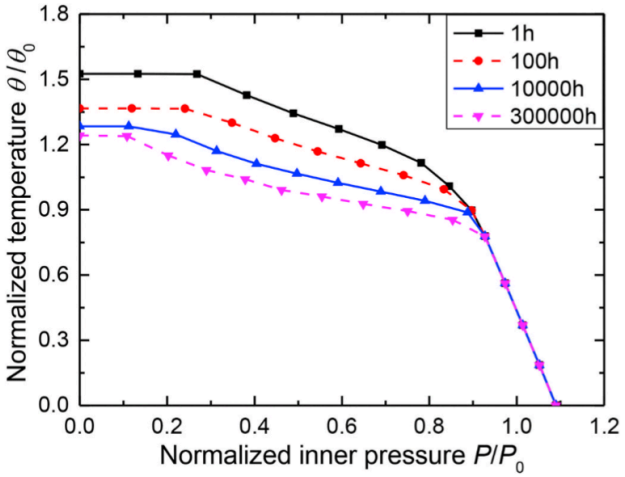

Fig. 8. Creep rupture limit interaction curves for the defect-free pipeline.

where δ_3 is an error margin. If Condition (16) is not satisfied, return to Step 1, and then the next iteration of outer loop starts. Otherwise, the outer loop iteration ends. The creep rupture limit factor λ_{creep} is obtained.

$$\lambda_{\text{creep}} = \lambda^{\text{limit}} \tag{17}$$

The numerical scheme described above has been incorporated into FE software of Abaqus [23] via the subroutines of UMAT and URDFIL in this work. The numerical scheme therefore becomes a general computational tool for creep rupture analysis and presents its applicability to complex geometry. It is noted that $\sigma_C(t_f, \theta(x_k))$ depends on the given rupture time t_f and temperature $\theta(x_k)$. After each iteration of outer loop, both the temperature $\theta(x_k)$ and the creep rupture strength $\sigma_C(t_f, \theta(x_k))$ at every material point are updated. The convergence and calculation accuracy of the numerical scheme have been described and discussed in Ref. [18].

3. Finite element model

3.1. Geometry and material

The geometric sketch of a pressure pipeline with volumetric defect under internal pressure and temperature load are shown in Fig. 1. To investigate the effect of geometrical configuration of part-through slots on the creep rupture limit load of pressure pipeline at elevated temperature, four types of geometric parameters of pressure pipeline with different sizes of part-through slots are considered (Table 1). The parameters R_i, R_o and L represent the inner radius, outer radius and length of the pressure pipeline, respectively. The parameters A, α and C determine the sizes of the part-through slot in three directions. The parameters A_1 and B represent the chamfer radii of part-through slot in axial and circumferential directions, respectively. In all cases, the same inner radius $R_i = 17$ mm, outer radius $R_o = 20$ mm and length $L = 250$ mm of the defective pipeline are chosen.

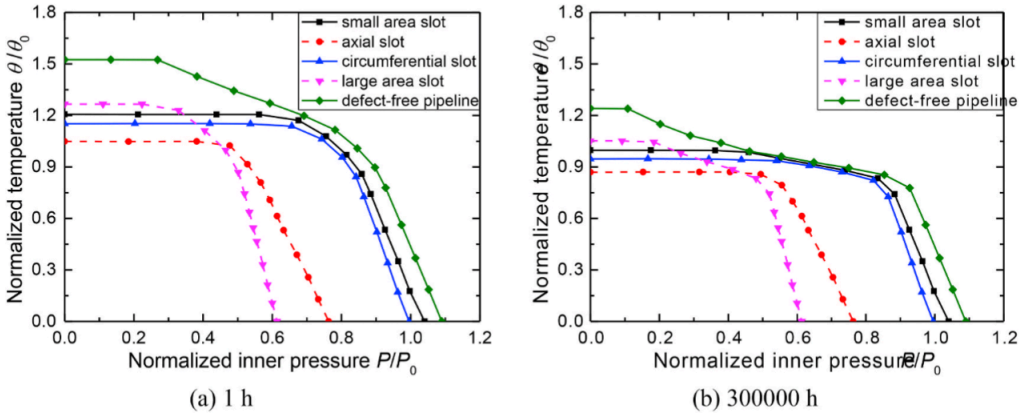

Fig. 9. Effect of part-through slots on the creep rupture limit interaction curves of defective pressure pipelines for creep rupture time (a) 1 h and (b) 300,000 h.

3.2. Material

The defective pipeline is made of 316 stainless steel material. According to the theory for creep rupture analysis, the creep rupture data required in Eqs. (4) and (5) are the key material parameters to determine the creep rupture limit of structure. Table 2 gives the relationship between creep rupture strength and temperature under different load holding times for 316 stainless steel [15]. It is noted that the creep rupture data are expressed as a series of discrete points at different temperatures and load holding times. The temperature range of creep rupture data given in Table 2 is from 425 °C to 800 °C, where 425 °C is the critical creep temperature. In FE analysis, the creep rupture strength between the two adjacent points is obtained by linear interpolation. Other material parameters used in the analysis are listed in Table 3. It can be found that for the temperature below 425 °C the modified yield strength used in Eq. (4) is decided by the original yield strength 445 MPa given in Table 3, and for the temperature above 425 °C the modified yield strength used in Eq. (4) is decided by the creep rupture strength given in Table 2.

3.3. Mesh

In this work, the Abaqus software in version of 6.14 [23] is utilised for FE analysis. The 20-node quadratic brick element (Abaqus type DC3D20) is adopted for heat transfer analysis, while the 20-node quadratic brick element with reduced integration technique (Abaqus type C3D20R) is adopted for structural stress analysis. Considering that these defective pipelines have two planes of symmetry, only one quarter section of the model is established for reducing the size of FE model. The FE meshes of defective pipelines with four types of part-through slots are displayed in Fig. 2. Gradient mesh seeds are set to optimise the mesh model, where dense meshes are used in the stress concentration zone and sparse meshes are used in the stress smooth zone. There are four layers of meshes in the thickness direction. The numbers of meshes for the pressure pipelines with small area slot, axial slot, circumferential slot, and large area slot are 1905, 1854, 1570, and 1834, respectively. These mesh models have been verified to satisfy the required accuracy of FE solution.

3.4. Load and boundary conditions

The defective pipeline is subjected to constant inner pressure and cyclic temperature field. The reference inner pressure is selected as $P_0 =$ 100 MPa. As shown in Fig. 3, the cyclic temperature history includes the temperature rise period A_1B_1, high temperature holding period B_1C_1, temperature fall period C_1D_1 and temperature rest period D_1A_2. For the high temperature holding period B_1C_1, the reference temperatures on the inward and outward surfaces of the defective pipeline are $\theta_{i0} =$ 600 °C and $\theta_{o0} =$ 450 °C, respectively, and the temperature is linearly distributed along the thickness. For the temperature rest period D_1A_2, the distribution of temperature field in the defective pipeline is uniform and below the creep temperature, which will lead to a zero stress state. The periods of temperature raise and fall are negligibly short compared to the temperature holding period. The creep deformation and creep damage of the pressure pipeline are inevitable during the temperature holding period. Because of only one quarter section of the model, the symmetric boundary conditions are applied to the two planes of symmetry. A uniform axial tension and the plane condition are applied to the end of the pressure pipeline to achieve the closed-end boundary condition. The uniform axial tension P_{T0} under the reference inner pressure P_0 is calculated by

$$P_{T0} = P_0 \frac{R_i^2}{R_o^2 - R_i^2} \tag{18}$$

In calculation of creep rupture limit, the entire reference temperature field θ_0 is scaled by a scaling factor.

4. Numerical calculation of creep rupture limit

For the combination of constant inner pressure and cyclic temperature load, there are two load vertices in a loading cycle. The linear FE analyses of the defective pressure pipeline under single inner pressure and single temperature load are respectively performed before carrying out the creep rupture analysis. Taking the pressure pipeline with a large area slot as an example, the FE solutions of the structure under the single reference inner pressure and the single reference temperature load are presented in Fig. 4(a) and (b). If the fictitious stress field of the defective pipeline under reference inner pressure is $\sigma_{ij}^E(x_k, P_0)$ and that under reference temperature field is $\sigma_{ij}^E(x_k, \theta_0)$, the linear elastic stress fields $\sigma_{ij}^E(x_k, t_1)$ and $\sigma_{ij}^E(x_k, t_2)$ at the two load vertices t_1 and t_2 are calculated by the means of superposition principle:

$$\sigma_{ij}^E(x_k, t_1) = \sigma_{ij}^E(x_k, P_0)\cos\varphi + \sigma_{ij}^E(x_k, \theta_0)\sin\varphi \tag{19}$$

$$\sigma_{ij}^E(x_k, t_2) = \sigma_{ij}^E(x_k, P_0)\cos\varphi \tag{20}$$

It is noted that the variation of φ $(0 \le \varphi \le \pi/2)$ corresponds to different ratios of inner pressure and temperature load. When φ changes from 0 to $\pi/2$, all possible ratios of inner pressure and temperature load can be covered.

The direct numerical approach is employed to carry out the creep rupture analysis. For each calculation of creep rupture limit, a specific value of φ is selected and then a load factor λ is output by the numerical approach procedure. The actual linear elastic stress fields at the two load

vertices are

$$\lambda\sigma_{ij}^{E}(x_k,t_1)=\lambda\sigma_{ij}^{E}(x_k,P_0)\cos\varphi+\lambda\sigma_{ij}^{E}(x_k,\theta_0)\sin\varphi \tag{21}$$

$$\lambda\sigma_{ij}^{E}(x_k,t_2)=\lambda\sigma_{ij}^{E}(x_k,P_0)\cos\varphi \tag{22}$$

It is important to note that the temperature field is also scaled by the load factor λ after each iteration of load factor, i.e. the actual temperature field $\theta(x_k)$ is

$$\theta(x_k)=\lambda\theta_0(x_k) \tag{23}$$

After obtaining the creep rupture limits within a series of ratios of inner pressure and temperature load, the creep rupture limit interaction curve is also determined. Fig. 5 displays the creep rupture limit interaction curve for the pressure pipeline with a large area slot under constant inner pressure and cyclic temperature load for the given creep rupture time 100 h.

To validate the obtained creep rupture limit interaction curve, a series of CBC analyses are conduct to test the cyclic plastic behaviors of the defective pipeline under load points on the either side of the curve. As shown in Fig. 5, six load points "R_1", "R_2", "C_1", "C_2", "L_1", "L_2" are selected as the test points, where "R_1", "C_1", "L_1" are located inside the curve and "R_2", "C_2", "L_2" are located outside the curve. The plastic strain magnitude histories of the pressure pipeline with a large area slot under the six selected load points are shown in Fig. 6. It is evident from Fig. 6 that for load points "R_1", "C_1", "L_1" the plastic strain magnitudes increase during the initial several load cycles, but afterwards, the plastic strain magnitudes go to be horizontal, which represents shakedown behavior. For load points "R_2", "C_2", the plastic strain magnitudes increase in every load cycle, and therefore the deformation accumulates and finally becomes large enough to cause the failure of structure after a number of cycles, which represents ratcheting behavior. For load point "L_2", the plastic strain magnitudes fluctuate around a steady value in every load cycle, but the accumulation of strains over these cycles is equal to zero, which represents alternating plasticity behavior. The transition of cyclic plastic behavior of the pressure pipeline with a large area slot for load points "R_1"/"C_1"/"L_1" and "R_2"/"C_2"/"L_2" verifies the correctness of the creep rupture limit interaction curve.

5. Results and discussions

The direct numerical approach is employed to carry out the creep rupture analyses for the pressure pipelines with four types of part-through slots and the defect-free pipeline under various combinations of constant inner pressure and cyclic temperature load. Four creep rupture times 1 h, 100 h, 10000 h, and 300000 h are considered.

5.1. Creep rupture limit interaction curves for different creep rupture times

The creep rupture limit interaction curves for the pressure pipelines with four types of part-through slots are displayed in Fig. 7 and that for the defect-free pipeline is displayed in Fig. 8. These creep rupture limit interaction curves provide helpful information for integrity assessment of pressure pipeline with volumetric defect under elevated temperature. For a group of inner pressure and temperature, one can evaluate the safety of the defective pipeline under a high-temperature holding time. If the load point is located inside the creep rupture limit interaction curve for the specific high-temperature holding time, the defective pipeline is safe, otherwise the creep rupture failure occurs. If the high-temperature holding time is given, one can evaluate the safety of the defective pipeline under a group of inner pressure and temperature. Furthermore, if the inner pressure or temperature is also given one can find the maximum permissible temperature or inner pressure according to the creep rupture limit interaction curve.

Each of the creep rupture limit interaction curve can be divided into three sections. The three sections correspond to different failure mechanisms: local creep rupture, global creep rupture and global plastic rupture, as shown in Fig. 7(a). It is evident from these curves in Fig. 7 that with the increase of creep rupture time, the creep rupture limits decrease in the sections of local creep rupture and global creep rupture but remain unchanged in the section of global plastic rupture. It can be explained as follows: In the sections of global creep rupture and local creep rupture, the temperature is above the critical creep temperature of 425 °C, and thus the modified yield strength in Eq. (5) is decided by the creep rupture strength. In the section of global plastic rupture, the temperature is below the critical creep temperature, and thus the modified yield strength in Eq. (5) is determined by the original yield strength. With the increase of creep rupture time, the creep rupture strength decreases. In the sections of global creep rupture and local creep rupture the modified yield strength in Eq. (5) is reduced, but in the section of global plastic rupture, the modified yield strength in Eq. (5) remains unchanged.

5.2. Effect of part-through slot on creep rupture limit interaction curve

The effects of part-through slots on the creep rupture limit interaction curves of defective pressure pipelines for creep rupture time 1 h and 300,000 h are respectively presented in Fig. 9(a) and (b). It is observed from Fig. 9(a) that for the defect-free pipeline and the pipelines with small area slot, circumferential slot, and axial slot, the creep rupture limit interaction curve is gradually narrowed. There is an obvious gap in the local creep rupture section of interaction curve between the defect-free pipeline and these defective pipelines. This indicates that the part-through slot significantly reduces the local creep rupture limit of pipeline because of stress concentration caused by slot. The pipeline with a large area slot has the maximum creep rupture limit in the section of local creep rupture because of the weakest stress concentration, but has the minimum creep rupture limit in the section of global plastic rupture because of the maximum volume of material removal. Similar results can be found from Fig. 9(b) in investigating the effect of part-through slots on the creep rupture limit interaction curves of defective pressure pipelines for creep rupture time 300,000 h.

6. Conclusions

In the present study, the creep rupture assessment of pressure pipelines with four different types of part-through slots, namely, small areas slot, axial slot, circumferential slot, and large area slot, subjected to cyclic thermo-mechanical loadings has been done using a direct numerical approach. The following concluding remarks have arisen:

1. The direct numerical approach succeeds in determining the creep rupture limits of pressure pipelines with four different types of part-through slots and thereby generating their creep rupture limit interaction curves. The results obtained by the direct numerical approach are verified by cycle-by-cycle analysis and show the good calculation accuracy of the approach.
2. The creep rupture limit interaction curve can be divided into three sections, which respectively correspond to the failure mechanisms of global creep rupture, global plastic rupture and local creep rupture. With the increase of creep rupture time, the creep rupture limits decrease in the sections of local creep rupture and global creep rupture because of the reduction of creep rupture strength, but the creep rupture limits in the section of global plastic rupture remain unchanged because of the occurrence of plastic failure.
3. For the defect-free pipeline and the pipeline with small area slot, circumferential slot, and axial slot, the creep rupture limit interaction curve is gradually narrowed. The part-through slot significantly reduces the local creep rupture limit of pipeline because of stress concentration caused by slot. For the four types of defective pipelines, the pipeline with a large area slot has the maximum creep

rupture limit in the section of local creep rupture because of the weakest stress concentration but has the minimum creep rupture limit in the section of global plastic rupture because of the maximum volume of material removal.

4. These results give the helpful information for in-service integrity assessment of defective pressure pipelines at elevated temperature, and demonstrate the applicability and application prospect of the direct numerical approach in solving questions relevant to design or life assessment of other engineering structures.

Author comment

This paper entitled "**Creep rupture assessment of cyclically heated 3D pressure pipelines with volumetric defects using a direct numerical approach**" authored by Heng Peng, Yinghua Liu, Haofeng Chen has been presented at ISSI2020 and selected for potential publication in **International Journal of Pressure Vessels and Piping** (IJPVP). The authors promise that this paper has not been previously published and it is also not being considered contemporaneously for publication elsewhere.

Declaration of competing interest

We declare that we have no known competing financial interests or personal relationships that can influence the work reported in this paper.

Acknowledgements

The authors are grateful for the supports provided by the National Key Research and Development Program of China (Grant No. 2017YFF0210704) and the National Natural Science Foundation of China (Grant No. 11672147).

References

[1] CNSMC, GB/T 19624 Safety Assessment of In-Service Pressure Vessels Containing Defects, 2019. Beijing.
[2] H.F. Chen, W.H. Chen, T.B. Li, J. Ure, On shakedown, ratchet and limit analyses of defective pipeline, J Press Vess-T Asme. 134 (2012).
[3] H.F. Chen, Y.H. Liu, Z.Z. Cen, B.Y. Xu, Numerical analysis of limit load and reference stress of defective pipelines under multi-loading systems, Int. J. Pres. Ves. Pip. 75 (1998) 105–114.
[4] Y.H. Liu, Z.Z. Cen, B.Y. Xu, Numerical limit analysis of cylindrical shells with part-through slots, Int. J. Pres. Ves. Pip. 64 (1995) 73–82.
[5] Y.H. Liu, Z.Z. Cen, H.F. Chen, B.Y. Xu, Plastic collapse analysis of defective pipelines under multi-loading systems, Int. J. Mech. Sci. 42 (2000) 1607–1622.
[6] S. Murakami, Y. Liu, M. Mizuno, Computational methods for creep fracture analysis by damage mechanics, Comput. Methods Appl. Mech. Eng. 183 (2000) 15–33.
[7] B. Dyson, Use of CDM in materials modeling and component creep life prediction, J. Pressure Vessel Technol. 122 (2000) 281–296.
[8] T.H. Hyde, L. Xia, A.A. Becker, Prediction of creep failure in aero engine materials under multi-axial stress states, Int. J. Mech. Sci. 38 (1996) 385–403.
[9] X.H. Du, Z. Jie, Y.H. Liu, Plastic failure analysis of defective pipes with creep damage under multi-loading systems, Int. J. Mech. Sci. 128 (2017) 428–444.
[10] X. Du, D. Liu, Y. Liu, Numerical limit load analysis of 3D pressure vessel with volume defect considering creep damage behavior, Math. Probl Eng. 2015 (2015) 1–13.
[11] J.L. Xue, C.Y. Zhou, X.F. Lu, X.C. Yu, Plastic limit load of Grade 91 steel pipe containing local wall thinning defect at high temperature, Eng. Fail. Anal. 57 (2015) 171–187.
[12] J.-L. Xue, C.-Y. Zhou, J. Peng, Ultimate creep load and safety assessment of P91 steel pipe with local wall thinning at high temperature, Int. J. Mech. Sci. 93 (2015) 136–153.
[13] N. Wang, H.Q. Liu, Limit load analysis of pressure structures containing pitting defects subjected to high temperature creep, Mater. Trans. 57 (2016) 501–506.
[14] R. Ainsworth, R5: assessment procedure for the high temperature response of structures 3, British Energy Generation Ltd, 2003.
[15] ASME. Boiler & pressure vessel code: an international code. Rules for Construction of Nuclear Facility Components, Division 1-Subsection NH. New York2013.
[16] H.F. Chen, M.J. Engelhardt, A.R.S. Ponter, Linear matching method for creep rupture assessment, Int. J. Pres. Ves. Pip. 80 (2003) 213–220.
[17] D. Barbera, H. Chen, Creep rupture assessment by a robust creep data interpolation using the Linear Matching Method, Eur. J. Mech. Solid. 54 (2015) 267–279.
[18] H. Peng, Y. Liu, H. Chen, Numerical schemes based on the stress compensation method framework for creep rupture assessment, Eur. J. Mech. Solid. 83 (2020) 104014.
[19] A.R.S. Ponter, M. Engelhardt, Shakedown limits for a general yield condition: implementation and application for a Von Mises yield condition, Eur. J. Mech. Solid. 19 (2000) 423–445.
[20] D. Barbera, H. Chen, Y. Liu, F. Xuan, Recent developments of the linear matching method framework for structural integrity assessment, J. Pressure Vessel Technol. 139 (2017), 051101-051109.
[21] H. Peng, Y. Liu, H. Chen, A numerical formulation and algorithm for limit and shakedown analysis of large-scale elastoplastic structures, Comput. Mech. 63 (2019) 1–22.
[22] H. Peng, Y. Liu, H. Chen, Shakedown analysis of elastic-plastic structures considering the effect of temperature on yield strength: theory, method and applications, Eur. J. Mech. Solid. 73 (2019) 318–330.
[23] Abaqus, Dassault systems, 2014, Version 6.14.